Wavelength Dependent Optical Force Aggregation of Gold Nanorods for SERS in a Microfluidic Chip

Silvie Bernatová,[1,‡,] Maria Grazia Donato,[2,‡] Jan Ježek,[1] Zdeněk Pilát,[1] Ota Samek,[1] Alessandro Magazzù,[2,†] Onofrio M. Maragò,[2,*] Pavel Zemánek,[1,*] Pietro G. Gucciardi[2]*

[1]Czech Academy of Sciences, Institute of Scientific Instruments, Kralovopolská 147, 61264 Brno, Czech Republic.

[2]CNR-IPCF, Istituto per i Processi Chimico-Fisici, V.le Stagno D'Alcontres 37, I-98158 Messina, Italy.

ABSTRACT. Optical printing of metal-nanoparticles-proteins complexes in microfluidic chips is of particular interest in view of the potential applications in biomolecular sensing by surface enhanced Raman spectroscopy (SERS). SERS-active aggregates are formed when the radiation pressure pushes the particle-protein complexes on an inert surface, enabling the ultrasensitive detection of proteins down to pM concentration in short times. However, the role of plasmonic resonances on the aggregation process is still not fully clear. Here, we study the aggregation velocity as a function of excitation wavelength and power. We use a model system consisting of complexes formed of gold nanorods featuring two distinct localized plasmon resonances bound with Bovine Serum Albumin (BSA). We show that the aggregation speed is remarkably accelerated by 300% or 30% with respect to off resonant case if the nanorods are excited at the

long-axis or minor-axis resonance, respectively. Power dependent experiments evidence a threshold below which no aggregation occurs, followed by a regime with linear increase of the aggregation speed. At powers exceeding 10 mW we observe turbulence, bubbling and remarkable one order increase of the aggregation speed. Results in the linear regime are interpreted in terms of a plasmon-enhanced optical force that scales as the extinction cross-section and determines the nanorods sticking probability. Thermo-plasmonic effects are invoked to describe the results at the highest powers. Finally, we introduce a method for the fabrication of functional SERS substrates on demand in a microfluidic platform that can serve as the detection part in microfluidic bioassays or lab-on-a-chip devices.

INTRODUCTION

The ability of surface enhanced Raman spectroscopy[1,2] (SERS) to detect extremely low concentrations of analytes, provides a wide range of applications in analytical, biomolecular and life science applications.[3-5] It is generally accepted that the largest part of the signal enhancement in SERS is connected with the excitation of localized surface plasmon (LSP) resonances in metal nanoparticles, also called optical nanoantennas.[6,7,8] According to the so-called the E^4 model,[9] the electromagnetic enhancement in SERS is due to a twofold effect in which metal nanoparticles excited at resonance are able to amplify both the excitation and the re-radiated field.[10,11] SERS is capable of single molecule sensitivity,[12] on both Raman-resonant and non-resonant molecules.[13] Generally accepted values of the enhancement factors[14] are up to 10^{10} with claims[15] ramping up to 10^{13}.

The SERS effect, first observed on molecules adsorbed on roughened silver surfaces,[16] is currently the subject of intense research. Nowadays different high efficiency substrates are

exploited, among which metallic nanostructured surfaces,[17-19] engineered nanoparticles and nanoantennas of different shapes,[20-22] colloidal nanoparticles,[23,24] or clusters of metal spheres.[25] Furthermore, magneto-plasmonic systems, such as noble metal nanoalloys, are acquiring increased importance[8] since they combine both plasmonic and magnetic properties that can be easily engineered by changing the doping fraction.[26] Recently, particle manipulation and aggregation by magnetic fields has also been achieved permitting the reversible assembling of aggregates and SERS hot-spots.[27]

Optical forces[28,29] and optical tweezers[30-32] have been exploited extensively for the manipulation, positioning, and aggregation of plasmonic nanoparticles.[33-37] At the nanoscale,[38] *i.e.*, for particles much smaller than the laser wavelength, optical forces can be well described in the dipole approximation.[39,40] For a focused laser beam, two main optical force components are identified:[29,31] the *gradient force*, which attracts particles towards the high-intensity focal spot, and the *scattering force*, that tends to push particles along the beam propagation direction. For the specific case of metal nanoparticles optical forces are further enhanced by the occurrence of plasmon resonances.[8,41-44] In particular, when the energy of the laser field is far-off the LSP resonance, optical forces are dominated by the gradient force that can either attract[45-48] or repel[40,49] nanoparticles from the high field intensity region. Thus, under suitable conditions, metal nanoparticles can be trapped in the focal region of an optical tweezers.[45-48] Instead, when the light is nearly-resonant with the particle LSP resonance, optical forces are dominated by radiation pressure[28] and can be used to efficiently and selectively[50] push nanoparticles along the beam optical axis onto a substrate.[51-57] In this context, optical forces have been applied to optically print nanoparticles into patterns of individual, or aggregated elements,[51,52,56] as well as of 2D-materials[58] on surfaces, such as glass or polymers.

Optical forces play an important role for SERS molecular detection in liquid environment. Svedberg et al.[59] were the first to optically create a SERS-active dimer of metal nanoparticles in liquid and to show the SERS-induced fingerprint of the thiophenol dispersed in the solution. Since then, optical manipulation together with thermo-phoretic effects[60] have been used to optically induce the creation of SERS-active aggregates of metal nanoparticles and detect dyes,[61,62] phenols,[63] proteins,[55-57] in liquid solutions and on different substrates (glass, polymers). Notably, the aggregation process is also reversible as soon as surface molecules are not used to tightly bind the particles to the substrate.[58,61] Using this approach single molecule sensitivity has been shown on resonant molecules of Rhodamine 6G/Nile Blue mixtures,[61] a pM sensitivity in the resonant detection of haemoglobin,[56] and down to 50 nM on non-resonant BSA molecules.[55]

A plasmonic enhancement of the optical forces has been observed in the trapping of colloidal aggregates,[43] whereas the role of the plasmon resonances on the optical pushing and aggregation process is not fully elucidated as both optical binding[64,65] and thermal effects[55] might play a role in the aggregation process. In this article, we investigate the aggregation dynamics of Bovine Serum Albumin (BSA) and gold nanorods (AuNRs) complexes as a function of wavelength and power. We observe that the aggregation process is remarkably accelerated when the nanoparticles are excited at resonance according to their extinction curve. Experiments as a function of power show that the optical aggregation is characterized by a threshold power, beyond which a linear increase of the aggregation speed with power is observed. For values of the optical power larger than 10 mW at the sample, we observe turbulence, bubbling, and an even higher aggregation velocity, that we attribute to thermoplasmonic effects. Finally, experiments are also carried out in an advanced microfluidic chip, suitable for SERS-based bimolecular detection applications.

MATERIALS AND METHODS

Gold nanorods. Commercial gold nanorods (Nanoseedz, 40 ± 3 nm diameter, 96 ± 7 nm length) are dispersed in DI water at a concentration 1.9×10^{10} particles/mL. The dispersion contains <0.1wt% Cetyltrimethylammonium bromide (CTAB) to prevent spontaneous re-aggregation.

Protein binding. Bovine Serum Albumin is purchased from Aldrich in lyophilized powder state. Protein buffered solutions are prepared by mixing the suitable amount of protein powder with a 200 mM of Phosphate Buffer solution (PB, pH 7.2). PB is prepared by dissolving Na_2HPO_4 (14.94 g) and NaH_2PO_4 (5.06 g) in 200 mL of DI water. Following this procedure we prepared samples containing BSA at concentrations of 10^{-4} M. The BSA-AuNRs solutions are prepared by mixing the nanorods with the proteins dissolved in PB in a volume ratio ranging from 1:7 v/v (AuNRs, BSA+PB). The solution is prepared and used at room temperature.

Extinction spectroscopy. Extinction spectra of the BSA-AuNR complexes are obtained by means of a Perkin Elmer L20 UV-Vis spectrophotometer.

Optical and Raman tweezers setups. The same microscope objective (Olympus UPLSAPO 60W, NA=1.2, WD=0.28 mm) has been used for all the measurements in different optical tweezers or Raman tweezers setups. The experimental setups were coupled to different laser sources, we give here details on each configuration depending on the wavelength used.

Aggregation and SERS signal growth has been studied at:

- **785 nm** employing a homemade Raman tweezers setup based on an inverted microscope configuration equipped with laser diode (Thorlabs DL7140-201S), notch filter (Semrock

Stopline NF03-785E-25) and spectrometer Horiba Triax 190 combined with Silicon Peltier-cooled CCD (Horiba).

- **561 nm** using a Horiba Jobin Yvon HR800 Raman micro-spectrometer in an upright microscope geometry equipped with laser Oxxius 561S-50-COL-PP.

Aggregation growth as a function of wavelength has been studied at the fixed power of 4 mW measured at the sample plane for each of the following wavelengths:

- **488 nm, 515 nm** from Ar^+ laser (MellesGriot , 543-AP-A01) coupled to Raman tweezers described above in *Aggregation and SERS signal growth*.
- **561 nm** from the HR800 setup discussed above in *Aggregation and SERS signal growth*.
- **633 nm** from He-Ne laser (JDSU 1145 P) coupled to Raman tweezers described above in *Aggregation and SERS signal growth*.
- **650 nm, 700 nm, 780 nm, and 840 nm** from a white light supercontinuum laser (SuperK Extreme, NKT Photonics) equipped with a variable bandpass filter (SuperKVaria, NKT Photonics) restricting the wavelength bandwidth to about 10 nm and coupled to an optical tweezers setup based on a Zeiss inverted microscope (Axiovert 100).

Aggregation as a function of power and aggregation in the microfluidic chip. We employed a homemade Raman tweezers (inverted microscope geometry) equipped with imaging spectrograph (SpectraPro2300i, PI Acton), liquid-nitrogen-cooled spectroscopic CCD camera (Spec-10:100BR/LN, Princeton Instruments, Acton), 785 nm laser diode (Sacher TEC-510-0785-1000, M^2=1.7), and three-axes nano-positioning stage (Mad City Labs, Nano-LP 200).

Microfluidic chip. The microfluidic chip is fabricated from poly(dimethyl)siloxane (PDMS) polymer by conventional soft lithography using master stamps based on negative SU-8 epoxy

photoresist deposited on a silicon substrate.[66,67] SU-8 is spin-coated on the silicon wafer, illuminated by a UV lamp through a mask, and developed. The masks for photolithographic patterning of SU-8 are fabricated by ink-jet printing on a transparent foil by a specialized company (Gatema, Brno, Czech Republic). PDMS mixture (base to curing agent ratio of 10:1) is then poured into a mold formed by the SU-8 master stamp on Si wafer at the bottom and a square frame machined from polycarbonate. After curing, the resultant PDMS device is peeled off from the mold and attached to a glass slide using standard oxygen plasma treatment. PDMS polymer was used because its properties such as bio-compatible (insoluble in water, nontoxic to cell etc.), gas permeable, transparent in visible range and high level of viscoelasticity that make it a suitable platform for biological studies.[68]

The chamber for the SERS studies is made of two microscope slides separated 100-150 μm using PDMS spacers. Three microfluidic channels, all of width 30 μm, are connected with the glass chamber. One is used to extract the SERS structures and clean the chamber, the other two serve as the delivery part for BSA-AuNRs or analytes to be detected.

RESULTS AND DISCUSSION

Optical force positioning and aggregation. Samples are prepared starting from commercial AuNRs with a length of 96 nm and a transverse size of 40 nm (see Figure 1a). Their extinction shows a main plasmon resonance at 700 nm (long axis) and lower plasmon resonance at 520 nm (short axis). The AuNRs are mixed with BSA (10^{-4} M) in a phosphate buffer solution (PB, 200 mM). Upon mixing, BSA molecules substitute the CTAB layer around the nanorods, creating BSA-AuNR complexes stable in time.[56] The extinction spectrum of the complexes (Figure 1a)

displays the two main resonances typical of the individual AuNR, with a few nanometre shift,[56] proving the stability of the complexes. In order to establish the best aggregation conditions in our microfluidic device (Figure 1b), we performed a series of first control measurements on a standard glass chamber, made by a microscope slide and a coverslip separated by a 120 μm spacer (Figure 1c). Approximately 10 μL of solution are loaded in the sample chamber. After sealing with nail polish, the chamber is ready for measurements. During our experiments we used two different setups depending on whether we want to monitor only the aggregate size as a function of time, wavelength and power, or if we also want to monitor the SERS signal during aggregation. Specifically, we exploit multi-wavelength optical tweezers coupled with a supercontinuum white light laser for the first purpose, and a Raman tweezers setup coupled with 561 nm and 785 nm lasers for the second purpose (Figure 1d). Optical pushing is carried out by focusing the laser radiation with a 60X water immersion objective towards the top surface of the glass liquid cell (Figure 1c). Here the BSA-AuNR complexes adhere due to the BSA sticking properties and aggregate. The size evolution is followed during irradiation by recording optical images using a CCD camera. Aggregates up to several microns are observed after some minutes (Figure1e). During optical aggregation, hot spots are formed giving origin to intense SERS emission from BSA. The evolution of SERS spectra is followed by collecting the backscattered Raman signal. After all control measurements have been made, the glass chamber was implemented into a polydimethylsiloxane (PDMS) microfluidic device with three fluid channels (Figure 1b).

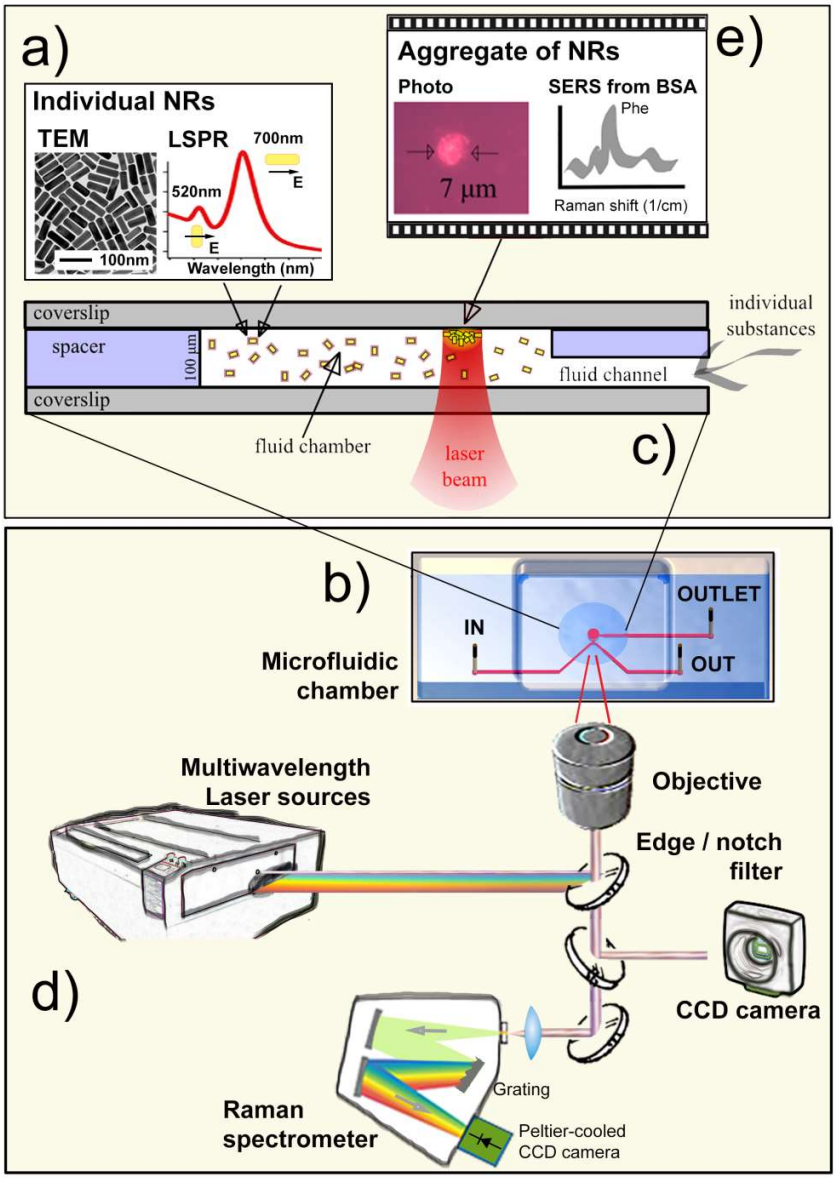

Figure 1. Sample properties and experimental setup. In (a) the TEM image and the extinction spectrum of the BSA-AuNR complexes are shown. In (b) the microfluidic chip is highlighted with a cross-section displayed in (c). (d) Simplified scheme of the Raman tweezers setup. Multiwavelength laser sources (white light supercontinuum, laser diodes, He-Ne, solid state, argon ions) are used. Upon laser focusing close to the chamber walls, optical aggregation of BSA-AuNR complexes is observed (e), with consequent observation of SERS emission.

Aggregate size and SERS signal growth. In order to study the dependence of both aggregate size and SERS enhancement of BSA as a function of pushing wavelength, we used two laser sources, emitting at 561 nm and 785 nm, close to the AuNRs plasmon resonances. We observed the aggregation process for each individual wavelength separately by recording CCD videos and by detecting Raman spectra at different times. The same laser beam was used for optical pushing and SERS excitation. The laser power was set at 5 mW at the sample plane in both cases. Each aggregation process was repeated several times in freshly prepared solutions. Five distinct aggregation evolution videos were analysed for each data set with fixed experimental parameters, while three distinct SERS signal evolution were analysed for each spectroscopic measurement. All data obtained from repeated experiments were fitted and the relevant parameters averaged over the independent measurements. The standard errors of each fitted parameters were obtained from the covariance matrix of the fit. The size of the aggregate was obtained by CCD images where the measured pixel size was converted to microns using a calibrating target. The aggregation process evolved in time (Figure 2a) for each individual wavelength. The evolution of the aggregate size is fitted with a Boltzmann growth kinetics equation[61] (solid lines in Figure 2a,b), given by:

$$f(t) = \frac{A_1 - A_2}{1+e^{(t-t_0)/\tau}} + A_2 \qquad (1)$$

where A_1, A_2 define the initial and final value of $f(t)$ at $t = -\infty$ and $t = \infty$, respectively. In our case we set A_1=0 because no process proceeds before laser starts illumination at t=0. The time t_0 denotes the value at which the size of aggregate reaches half of its maximum, $f(t_0) = (A_1 + A_2)/2$, and τ is connected to the slope of the curve at t_0. By fitting the curves obtained when pushing at 561 nm, we obtain τ=390±70 s, t_0=600±70 s, A_2=5700±300 nm, where the

uncertainties represent the standard error of the mean obtained from the covariance matrix of the fits of five independent data sets. By fitting the curve for 785 nm pushing we obtain τ=410±60 s, t_0=590±60 s, A_2=8300±300 nm. Except for the maximal values A_2, both processes follow a similar dynamics within the detected uncertainty.

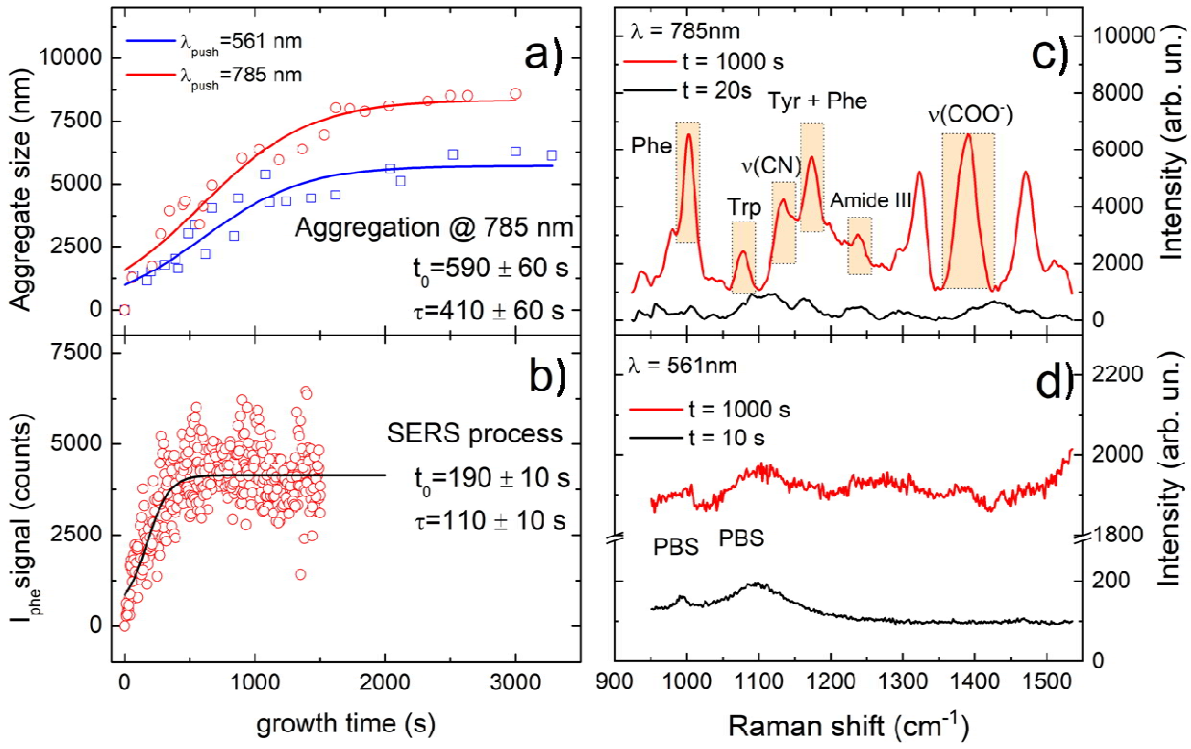

Figure 2. Temporal evolution of BSA-AuNR complexes aggregation and SERS processes. (a) Growth curves of the aggregate size for two different wavelengths, 561 nm and 785 nm. Data points correspond to aggregate size as measured from calibrated CCD images. (b) Growth of the SERS enhanced phenylalanine Raman peak (at 1002 cm^{-1}) at 785 nm excitation wavelength. Solid lines in (a) and (b) are the fit to the data with Equation 1, fitted parameters t_0 and τare also indicated. (c) Raman spectra obtained after 20 s and 1000 s at 785 nm excitation wavelength. After 1000 s the SERS enhanced spectrum of BSA is clearly visible. The peaks connected to

phenylalanine ring breathing (at ~1002 cm^{-1}), to CN and COO^- stretching vibrations (at ~1130 cm^{-1} and ~1396 cm^{-1}, respectively), to tryptophan (~1070 cm^{-1}) and tyrosine+phenylalanine (~1170 cm^{-1}) modes, and to the Amide III band (at ~1238 cm^{-1}) are easily recognized.[55](d) Raman spectra obtained at 561 nm excitation wavelength after 10 s and 1000 s aggregation time. Here only the low intensity peak of the phosphate buffer, PB, is visible, while BSA peaks are not visible because we are off resonance with respect to the AuNRs main plasmon peak at 700 nm and are overwhelmed by background fluorescence.

A similar study can be carried out also for the time evolution of the BSA SERS signal from hot-spots induced by the aggregates.[55] However, in the case of 561 nm laser excitation, Raman bands of BSA were not visible because we are off resonance with respect to the AuNRs main plasmon peak at 700 and they are overwhelmed by background fluorescence (Figure 2d). On the contrary, in the case of 785 nm laser excitation, we were able to resonantly enhance the BSA Raman bands that are clearly distinguishable from the background (Figure 2c). Among these, the phenylalanine peak intensity at approximately 1002 cm^{-1} was followed as a function of the excitation time, as reported in Figure 2b. The fit of the phenylalanine peak data with Equation 1 points out a different growth kinetic with respect to the aggregation process. In fact, this is due to the Raman signal saturation occurring when the sampling volume on the substrate (where the SERS signal generates) is completely filled with BSA-AuNR complexes, even if the aggregate continues to grow. Results shown in Figure 2 point out that the minimum aggregate size to obtain a saturated Raman signal is approximately 3 μm which is about four times larger than the diameter of the beam focus.

Wavelength and power dependence. In order to characterize the aggregate dynamics, the aggregation process has been carried out also using different pushing wavelengths. We define the

average velocity of aggregation, $\langle V_{aggr} \rangle$, as the ratio between the size of the aggregate and the corresponding time of aggregation in the linear regime, *i. e.*, before saturation. Each $\langle V_{aggr} \rangle$ value was obtained by averaging at least three independent aggregation processes. The evolution of the aggregate growth was always measured during the linear growing regime, before its saturation (Figure 2a). The beam power has been fixed at 4 mW for each wavelength. The aggregation process was monitored continuously by a CCD camera. Thus, at intervals of about 300-800 s the laser beam was blocked and the CCD image of the aggregate (see Figure 3a,b) was used to determine the actual aggregate size, providing the time evolution of the aggregate sizes and aggregation velocity (see also Supporting Information).

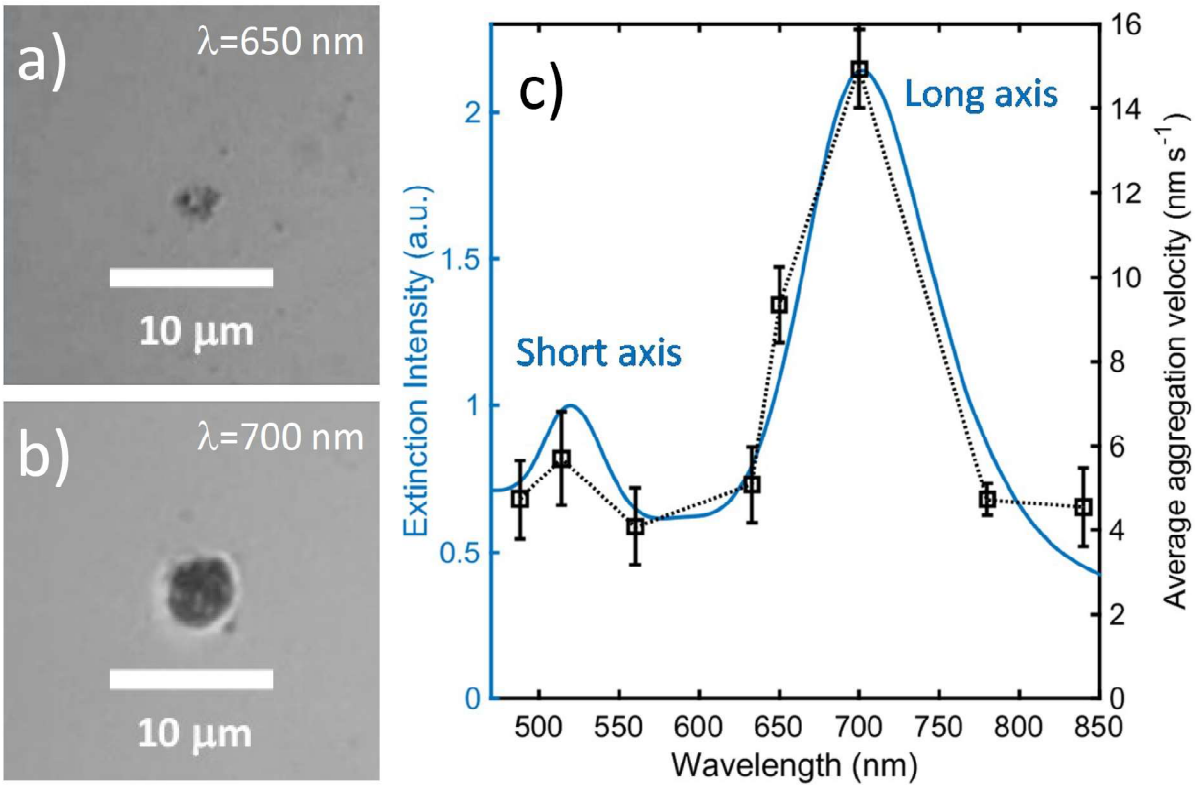

Figure 3. (a,b) CCD images of BSA-AuNRs aggregates after 500 s of optical pushing with 4 mW of power at the sample. In (a) the aggregation is obtained with a wavelength of 650 nm,

away from the plasmon resonance, and an aggregate size of about 2 μm is measured. In (b) a wavelength of 700 nm, close to the AuNRs plasmon resonance, has been used in the same experimental conditions obtaining an aggregate size of about 6 μm. (c) AuNRs extinction spectrum (solid blue line) and average velocity of aggregation $<V_{aggr}>$ (black squares). The two peaks correspond to the short and long axis localized surface plasmon resonances. The uncertainties on the aggregation velocity data represent the standard deviation of the mean over five independent measurements. The agreement between the wavelength dependence of the two curves is very good showing that for low power (<10 mW) the scattering force, proportional to the extinction cross section, controls the AuNRs dynamics.

In Figure 3 it is clearly observed that the average aggregation velocity follows the extinction spectrum of the plasmonic nanoparticles. This indicates that the force driving the pushing process is essentially the scattering force, which is directly connected to the extinction cross-section,[31,32] σ_{ext} (see Supporting Information). The calculation of optical forces in the dipole approximation[39,40] agrees well with this scenario (see Supporting Information). This approximation is generally valid for particles much smaller than the laser wavelength, such as our AuNRs, giving reasonable insights on the mechanical effects of light on nanoparticles.[31,44] In general to calculate the total optical force both the gradient force, proportional to the real part of the particle polarizability, and the scattering force, proportional to the extinction cross section, need to be considered (see Supporting Information). However, in our case the total optical force is mostly coincident with the scattering force, F_{scatt}, except for wavelengths in the near infrared region where the gradient force is of the same order of magnitude of the scattering force (see curves at 800 nm in Figure S1e of the Supporting Information) and hence the proportionality with the extinction cross section might be less evident. However, even in this case, the total

optical force is always positive, namely, directed towards the substrate, driving the aggregation process. The largest values of the scattering force (approximately 1 pN) is obtained in proximity of the plasmon resonance at the wavelength of 700 nm and at the laser focus where the scattering force is easily expressed as $F_{scatt}=2n_m\sigma_{ext}P/\pi cw_0^2$ in terms of the medium refractive index, n_m, light velocity in vacuum, c, extinction cross section, σ_{ext}, and Gaussian beam waist, w_0 (see Supporting Information).

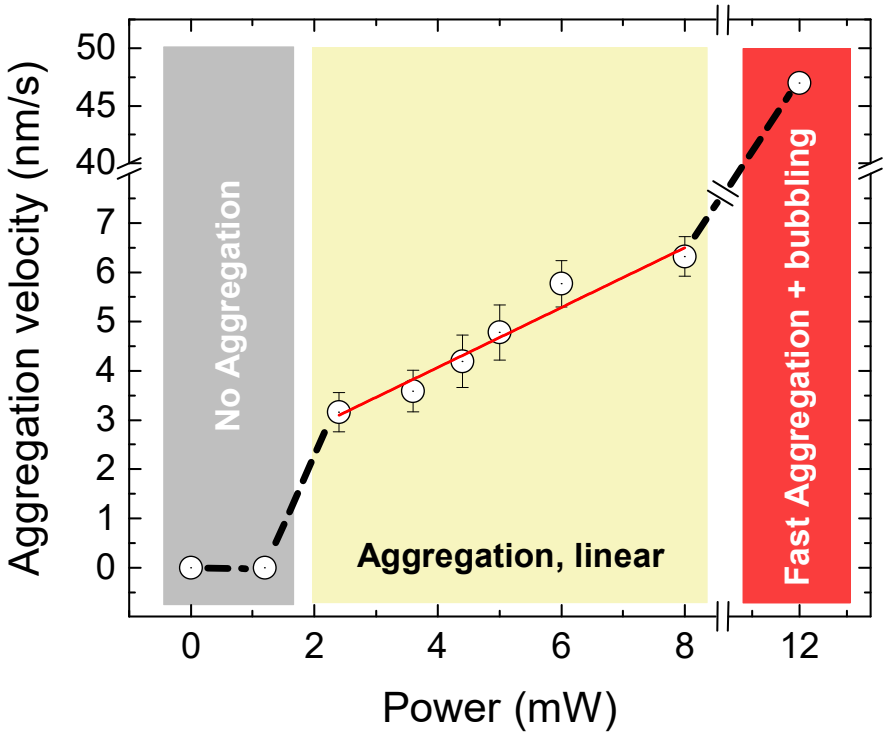

Figure 4. Aggregation velocity (white circles) as a function of pushing laser power at the wavelength 785 nm. Three different regimes are outlined: no aggregation up to 2.4 mW, a linear regime (red line is a fit with a slope 618±4 nm $s^{-1}W^{-1}$) up to 8 mW, and finally a chaotic regime at 12 mW. The black dashed line is a guide to the eye.

The linear dependence of the average aggregation velocity on the laser power, P, is experimentally verified at 785 nm laser wavelength in Figure 4, where we also observe that the

minimum laser power required to obtain aggregation is 2.4 mW. At lower power, aggregation is not observed. This linear dependence of the aggregation velocity with power is a direct consequence of the balance between the scattering force and the Stokes' force, $F_{scatt} \approx F_{Stokes}$, in the nanorods dynamics in liquid. In fact, the aggregation velocity is proportional to the nanorods drift velocity in the Gaussian laser beam that at low Reynolds numbers is estimated as $v_{drift} \approx F_{scatt}/\gamma$, where γ is the nanorod viscous damping in water. Hence we have that the nanorod drift velocity is proportional to laser power and close to the focal spot we have that $v_{drift} \approx 2n_m \sigma_{ext} P/\pi\gamma c w_0^2$. As a consequence, in this regime, also the aggregation velocity has a linear dependence with laser power. This holds for a laser power above the activation threshold and as soon as the laminar flow is not broken. In fact, increasing the beam power over 10 mW at the sample, we observe the occurrence of a nonlinear regime where the aggregation becomes very fast, inducing strong thermal effects and bubbling after few seconds.

The process described above has been implemented on a microfluidic chip to demonstrate its direct applicability in situ within a microfluidic bioassay or in a lab-on-a-chip device. The chip body is made of poly(dimethyl)siloxane (PDMS), the microfluidic channels lead to the aggregation chamber which is placed in between two microscope slides, as shown in Figure 5. BSA-AuNR complexes were delivered through one inlet to the micro-chamber. Alternatively they can be prepared directly in the micro-chamber using both inlets, one for BSA the second for AuNRs. When the micro-chamber is filled with BSA-AuNR, the flow was stopped and 785 nm laser beam was focused on the top of coverslip of the micro-chamber to aggregate the AuNR and initiate SERS emission. The Raman spectra collected at 10 s and 1000 s of the aggregation process are shown in Figure 5d and prove very good reproducibility. Many SERS active areas were prepared in the micro-chamber by repositioning the microscope stage and focusing the laser

to a new area of the micro-chamber. The used SERS active structures were drained out from the micro-chamber via the outlet channel and new structures were built up by re-focusing the laser on the micro-chamber surface. By comparing Figure 5d and 2c we note that we have very good reproducibility between the spectra obtained using the chip and the control measurements performed in the standard glass chamber, despite the fact that different experimental setups have been used (see Materials and Methods). Such microfluidic platform enables multiple and repeatable in situ fabrication of SERS substrates in the chip chamber and various analytes can be analysed in the same chip.

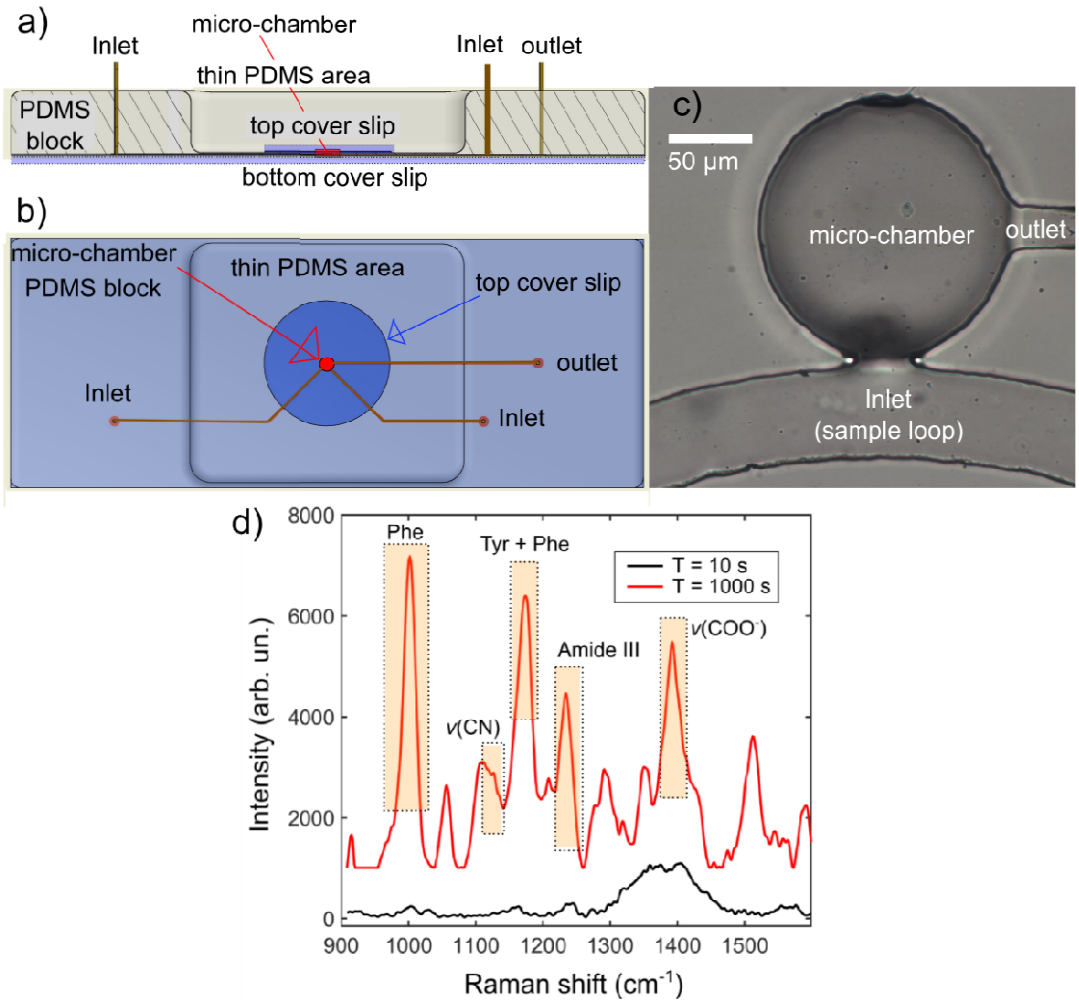

Figure 5. Schematic design of the microfluidic chipwhich consists of two parts, a glass micro-chamber, red parts in (a) and (b), and delivery parts for fluid and samples, brown lines. Inlet delivers the substances to the micro-chamber (sample loop) and the used sample is drained out the micro-chamber by the outlet. (a) A cross section of the chip, side view. (b) An overall top view of the chip. (c) A microscope image (top view) of the micro-chamber of depth 100-150 μm. (d) Raman spectrum from an aggregate prepared directly in the microfluidic chip after 10 s (black) and 1000 s (red). The main Raman signatures of BSA are highlighted in the SERS enhanced spectrum (red).

CONCLUSIONS

In this work we showed a novel procedure to obtain SERS-active hotspots directly inside a microfluidic chip. Optical forces have been used to create aggregates of metal nanoparticles (AuNRs) in presence of molecular species, increasing their Raman signal over their ordinary limit of detection. We used the above procedure to detect BSA in 10^{-4} M concentration, which is under the limit of detection of standard Raman spectroscopy. The growth kinetics of the optically induced aggregates has been studied, showing that it is possible to aggregate nanorods in a confined region having size in the 2-10 μm size and in a few hundred seconds. Moreover, it has been shown that the average aggregation velocity follows the extinction spectrum of AuNRs, which is a valuable information for the design of SERS sensors with plasmonic particles of different size, shape, and composition. The application of the above procedure directly inside a microfluidic device, in sterile conditions and without any outside intervention, paves the way to a new concept of biosensor, operating *in situ* in the natural environment of biomolecules.

ASSOCIATED CONTENT

Supporting Information is available free of charge on the ACS Publications website. Optical forces on gold nanorods in the dipole approximation, white light supercontinuum laser source (PDF).

AUTHOR INFORMATION

Corresponding Author

*Email: berns@isibrno.cz; onofrio.marago@cnr.it; zemanek@isibrno.cz

Present Addresses

†Department of Physics, University of Gothenburg, SE-41296 Gothenburg, Sweden.

Author Contributions

The manuscript was written through contributions of all authors. All authors have given approval to the final version of the manuscript.

‡These authors contributed equally.

ACKNOWLEDGMENT

We acknowledge financial support by the Joint Bilateral Project CNR-16-12 between the Italian National Research Council (CNR) and the Czech Academy of Sciences (CAS), the COST Action "Raman4Clinics", and project MEYS CR LO1212.

REFERENCES

(1) Moskovits, M. Surface-Enhanced Spectroscopy. *Rev. Mod. Phys.***1985**, *57*, 783.

(2) Le Ru, E. C.; Etchegoin, P. G. *Principles of Surface-Enhanced Raman Spectroscopy: And Related Plasmonic Effects;* Elsevier: Amsterdam, 2009.

(3) Lamy de La Chapelle, M. *Handbook of Enhanced Spectroscopy*, CRC Press, 2015.

(4) Prochaska, M. *Surface Enhanced Raman Spectroscopy*,Springer 2016.

(5) Schluecker, S. *Surface Enhanced Raman Spectroscopy*, Wiley, 2011.

(6) Maier, S. A. *Plasmonics: Fundamentals and Applications*; Springer, New York, 2007.

(7) Muehlschlegel, P.; Eisler, H. J.; Martin, O. J.; Hecht, B.; Pohl, D. W. Resonant Optical Antennas. *Science* **2005**, *308*, 1607-1609.

(8) Amendola, V.; Pilot, R.; Frasconi, M.; Marago, O. M.; Iati, M.A. Surface Plasmon Resonance in Gold Nanoparticles: A Review. *Journal of Physics: Condensed Matter* **2017**, *29*, 203002.

(9) Le Ru, E. C.; P. G. Etchegoin. Rigorous Justification of the $|E|^4$ Enhancement Factor in Surface Enhanced Raman Spectroscopy. *Chem. Phys. Lett.* **2006**, *423*, 63-66.

(10) Guillot, N.; Lamy de la Chapelle, M. The Electromagnetic Effect in Surface Enhanced Raman Scattering: Enhancement Optimization Using Precisely Controlled Nanostructures. *J. Quant. Spectr. Rad. Transf.* **2012**, *113*, 2321-2333.

(11) Fazio, B.; D'Andrea, C.; Bonaccorso, F.; Irrera, A.; Calogero, G.; Vasi, C.; Gucciardi, P. G.; Allegrini, M.; Toma, A.; Chiappe, D.; et al. Re-radiation Enhancement in Polarized Surface-Enhanced Resonant Raman Scattering of Randomly Oriented Molecules on Self-Organized Gold Nanowires. *ACS Nano* **2011**, *5*, 5945-5956.

(12) Shuming, N.; Emory, S. R. Probing Single Molecules and Single Nanoparticles by Surface-Enhanced Raman Scattering. *Science* **1997**, *275*, 1102-1106.

(13) Zrimsek, A. B.; Chiang, N.; Mattei, M.; Zaleski, S.; McAnally, M. O.; Chapman, C. T.; Henry, A. I.; Schatz, G. C.; Van Duyne, R. P. Single-Molecule Chemistry with Surface and Tip-Enhanced Raman Spectroscopy. *Chemical Reviews* **2017**, *117*, 7583-7613.

(14) Le Ru, E.C.; Blackie, E.; Meyer, M.; Etchegoin, P.G. Surface Enhanced Raman Scattering Enhancement Factors: A Comprehensive Study. *J. Phys. Chem. C* **2007**, *111*, 13794-13803.

(15) Wang, D.; Zhu, W.; Best, M. D.; Camden, J. P.; Crozier, K. B. Directional Raman Scattering from Single Molecules in the Feed Gaps of Optical Antennas. *Nano Letters* **2013**, *13*, 2194−2198.

(16) Fleischmann, P.; Hendra, P. J.; McQuilla A. J. Raman Spectra of Pyridine Adsorbed at a Silver Electrode. *Chem. Phys. Lett.* **1974,** *26*,163-166.

(17) Moskovits, M. Surface-Enhanced Raman Spectroscopy: A Brief Retrospective. *J. Ram. Spec.* **2005,** *36*, 485-496.

(18) Halas, N. J.; Moskovits, M. Surface-Enhanced Raman Spectroscopy: Substrates and Materials for Research and Applications. *MRS Bulletin* **2013,** *38*, 607-614.

(19) Balint, S.; Kreuzer, M. P.; Rao, S.; Badenes, G.; Miskovsky, P.; Petrov. D. Simple Route for Preparing Optically Trappable Probes for Surface-Enhanced Raman Scattering. *J. Phys. Chem. C* **2009**, *113*, 17724-17729.

(20) Le, F.; Brandl, D. W.; Urzhumov, Y. A.; Wang, H.; Kundu, J.; Halas, N. J.; Aizpurua, J.; Nordlander, P. Metallic Nanoparticle Arrays: A Common Substrate for Both Surface-Enhanced Raman Scattering and Surface-Enhanced Infrared Absorption. *ACS Nano* **2008,** *2*, 707-718.

(21) D'Andrea, C.; Bochterle, J.; Toma, A.; Huck, C.; Neubrech, F.; Messina, E.; Fazio, B.; Marago, O. M.; Di Fabrizio, E.; Lamy de La Chapelle, M.; et al. Optical Nanoantennas for Multiband Surface-Enhanced Infrared and Raman Spectroscopy. *ACS Nano* **2013**, *7*, 3522-3531.

(22) D'Andrea, C.; Fazio, B.; Gucciardi, P. G.; Giordano, M. C.; Martella, C.; Chiappe, D.; Toma, A.; Buatier de Mongeot, F.; Tantussi, F.; Vasanthakumar, P.; et al. SERS Enhancement and Field Confinement in Nanosensors Based on Self-Organized Gold Nanowires Produced by Ion-Beam Sputtering. *J. Phys. Chem. C* **2014**, *118*, 8571-8580.

(23) Indrasekara, A. D. S.; Meyers, S.; Shubeita, S.; Feldman, L. C.; Gustafsson, T.; Fabris, L. Gold Nanostar Substrates for SERS-Based Chemical Sensing in the Femtomolar Regime. *Nanoscale* **2014**, *6*, 8891-8899.

(24) Hering, K.; Cialla, D.; Ackermann, K.; Dörfer, T.; Möller, R.; Schneidewind, H.; Mattheis, R.; Fritzsche, W.; Rösch, P.; Popp, J. SERS: A Versatile Tool in Chemical and Biochemical Diagnostics. *Analytical and Bioanalytical Chemistry* **2008**, *390*, 113-124.

(25) Lee,S. J.; Morrill, A. R.; Moskovits, M. Hot Spots in Silver Nanowire Bundles for Surface-Enhanced Raman Spectroscopy. *J. Amer. Chem. Soc*. **2006,** *128*, 2200-2201.

(26) Amendola, V.; Saija, R.; Maragò, O. M.; Iatì, M. A. Superior Plasmon Absorption in Iron-Doped Gold Nanoparticles. *Nanoscale* **2015**, *7*, 8782-8792.

(27) Scaramuzza, S.; Badocco, D., Pastore, P., Coral, D. F., Fernández van Raap, M. B.; Amendola, V. Magnetically Assembled SERS Substrates Composed of Iron–Silver Nanoparticles Obtained by Laser Ablation in Liquid. *Chem. Phys. Chem.* **2017**, *18*, 1026-1034.

(28) Ashkin, A. Acceleration and Trapping of Particles by Radiation Pressure. *Phys. Rev. Lett.***1970,** *24*, 156–159.

(29) Jonáš, A.; Zemánek, P. Light at Work: The Use of Optical Forces for Particle Manipulation, Sorting, and Analysis. *Electrophoresis* **2008**, *29*, 4813–4851.

(30) Ashkin, A.; Dziedzic, J. M.; Bjorkholm, J. E.; Chu, S. Observation of a Single-Beam Gradient Force Optical Trap for Dielectric Particles. *Opt. Lett.* **1986,** *11*, 288–290.

(31) Polimeno, P.; Magazzù, A.; Iatì, M. A.; Patti, F.; Saija, R.; Degli Esposti Boschi, C.; Donato, M. G.; Gucciardi, P. G.; Jones, P. H.; Volpe, G.; et al. Optical Tweezers and Their Applications. *J. Quant. Spectr. Rad. Transf.* **2018**, *218*, 131–150.

(32) Jones, P. H.; Maragò, O. M.; Volpe, G. *Optical Tweezers: Principles and Applications*; Cambridge University Press, Cambridge, 2015.

(33) Gargiulo, J.; Cerrota, S.; Cortés, E.; Violi, I. L.; Stefani, F. D. Connecting Metallic Nanoparticles by Optical Printing. *Nano Letters* **2016,** 16,1224-1229.

(34) Do, J.; Fedoruk, M.; Jäckel, F.; Feldmann, J. Two-Color Laser Printing of Individual Gold Nanorods. *Nano Letters* **2013,** 13, 4164-4168.

(35) Fedoruk, M.; Meixner, M.; Carretero-Palacios, S.; Lohmüller, T.; Feldmann, J. Nanolithography by Plasmonic Heating and Optical Manipulation of Gold Nanoparticles *ACS Nano* **2013**, *7*, 7648-7653.

(36) Do, J.; Schreiber, R.; Lutich, A. A.; Liedl, T.; Rodríguez-Fernández, J.; Feldmann, J. Design and Optical Trapping of a Biocompatible Propeller-like Nanoscale Hybrid. *Nano Letters* **2012,** *12*, 5008-5013.

(37) Gargiulo, J.; Violi, I. L.; Cerrota, S.; Chvátal, L.; Cortés, E.; Perassi, E. M.; Diaz, F.; Zemánek, P.; Stefani, F. D. Accuracy and Mechanistic Details of Optical Printing of Single Au and Ag Nanoparticles *ACS Nano* **2017,** *11*, 9678-9688.

(38) Maragò, O.M.; Jones, P.H.; Gucciardi, P.G.; Volpe, G.; Ferrari, A.C. Optical Trapping and Manipulation of Nanostructures. *Nat. Nanotechnol.* **2013,** *8*, 807–819.

(39) Chaumet, P.; Nieto-Vesperinas, M. Time-Averaged Total Force on a Dipolar Sphere in an Electromagnetic Field. *Opt. Lett.* **2000**, *25*, 1065.

(40) Arias-González, J. R.; Nieto-Vesperinas, M. Optical Forces on Small Particles: Attractive and Repulsive Nature and Plasmon Resonance Conditions. *J. Opt. Soc. Am. A* **2003,** *20*, 1201–1209.

(41) Urban, A. S.; Carretero-Palacios, S.; Lutich, A. A.; Lohmüller, T.; Feldmann, J.; Jäckel, F. Optical Trapping and Manipulation of Plasmonic Nanoparticles: Fundamentals, Applications, and Perspectives. *Nanoscale* **2014,** *6*, 4458–4474.

(42) Hongxing, X.; Käll, M. Surface-Plasmon-Enhanced Optical Forces in Silver Nanoaggregates. *Phys. Rev. Lett.* **2002,** *89*, 246802.

(43) Messina, E.; Cavallaro, E.; Cacciola, A.; Iatì, M. A.; Gucciardi, P. G.; Borghese, F.; Denti, P.; Saija, R.; Compagnini, G.; Meneghetti, et al. Plasmon-Enhanced Optical Trapping of Gold Nanoaggregates with Selected Optical Properties. *ACS Nano* **2011,** *5*, 905–913.

(44) Messina, E.; Donato, M.; Zimbone, M.; Saija, R.; Iatì, M.; Calcagno, L.; Fragalà, M.; Compagnini, G.; D'Andrea, C.; Foti, A.; et al. Optical Trapping of Silver Nanoplatelets. *Opt. Express* **2015,** *23*, 8720–8730.

(45) Svoboda, K.; Block, S. M. Optical Trapping of Metallic Rayleigh Particles. *Opt. Lett.* **1994,** *19*, 930–932.

(46) Selhuber-Unkel, Ch.; Zins, I.; Schubert, O.; and Sönnichsen, C.; Oddershede, L. B. Quantitative Optical Trapping of Single Gold Nanorods. *NanoLett.* **2008,** *8*, 2998–3003.

(47) Brzobohatý, O.; Šiler, M.; Trojek, J.; Chvátal, L.; Karásek, V.; Paták, A.; Pokorná, Z.; Mika, F.; Zemánek, P. Three-Dimensional Optical Trapping of a Plasmonic Nanoparticle Using Low Numerical Aperture Optical Tweezers. *Sci. Rep.* **2015,** *5*, 8106.

(48) Messina, E.; D'Urso, L.; Fazio, E.; Satriano, C.; Donato, M. G.; D'Andrea, C.; Maragò, O. M.; Gucciardi, P.G.; Compagnini, G.; Neri, F. Tuning the Structural and Optical Properties of Gold/Silver Nano-Alloys Prepared by Laser Ablation in Liquids for Optical Limiting, Ultra-Sensitive Spectroscopy, and Optical Trapping. *Journal of Quantitative Spectroscopy and Radiative Transfer* **2012**, *113*, 2490-2498.

(49) Dienerowitz, M.; Mazilu, M.; Reece, P. J.; Krauss, T. F.; Dholakia, K. Optical Vortex Trap for Resonant Confinement of Metal Nanoparticles. *Opt. Express* **2008,** *16*, 4991–4999.

(50) Ploschner, M.; Cizmar, T.; Mazilu, M.; Di Falco, A.; Dholakia, K. Bidirectional Optical Sorting of Gold Nanoparticles. *Nano Lett.* **2012**, *12*, 1923-1927.

(51) Nedev, S.; Urban, A. S.; Lutich, A. A.; Feldmann, J. Optical Force Stamping Lithography. *Nano Lett.* **2011,** *11*, 5066–5070.

(52) Guffey, M. J.; Scherer, N. F. All-Optical Patterning of Au Nanoparticles on Surfaces Using Optical Traps. *Nano Lett.* **2010,** *10*, 4302–4308.

(53) Königer, A.; Köhler, W. Optical Funneling and Trapping of Gold Colloids in Convergent Laser Beams. *ACS Nano* **2012**, *6*, 4400–4409.

(54) Li, M.; Lohmueller, T.; Feldmann, J. Optical Injection of Gold Nanoparticles into Living Cells. *Nano Lett.* **2015**, *15*, 770–775.

(55) Fazio, B.; D'Andrea, C.; Foti, A.; Messina, E.; Irrera, A.; Donato, M.G.; Villari, V.; Micali, N.; Maragò, O.M.; Gucciardi, P.G. SERS Detection of Biomolecules at Physiological pH via Aggregation of Gold Nanorods Mediated by Optical Forces and Plasmonic Heating. *Sci. Rep.* **2016**, *6*, 26952.

(56) Foti, A.; D'Andrea, C.; Villari, V.; Micali, N.; Donato, M.G.; Fazio, B.; Maragò, O.M.; Gillibert, R.; Lamy de la Chapelle, M.; Gucciardi, P.G. Optical Aggregation of Gold Nanoparticles for SERS Detection of Proteins and Toxins in Liquid Environment: Towards Ultrasensitive and Selective Detection. *Materials* **2018**, *11*, 440.

(57) Donato, M. G.; Rajamanickam, V. P.; Foti, A.; Gucciardi, P. G.; Liberale, C.; Maragò, O. M. Optical Force Decoration of 3D Microstructures with Plasmonic Particles, *Opt. Lett.* **2018,** *43*, 5170-5173.

(58) Donato, M. G.; Messina, E.; Foti, A.; Smart, T. J.; Jones, P. H.; Iatì, M. A.; Saija, R.; Gucciardi, P. G.; Maragò, O.M. Optical Trapping and Optical Force Positioning of Two-Dimensional Materials. *Nanoscale* **2018**, *10*, 1245-1255.

(59) Svedberg, F.; Li, Z.; Xu, H.; Käll, M. Creating Hot Nanoparticle Pairs for Surface-Enhanced Raman Spectroscopy through Optical Manipulation. *Nano Lett.* **2006**, *6*, 2639–2641.

(60) Baffou, G.; Quidant, R. Thermo-Plasmonics: Using Metallic Nanostructures as Nano-Sources of Heat. *Laser Photon. Rev.* **2013**, *7*, 171–87.

(61) Patra, P. P.; Chikkaraddy, R.; Tripathi, R. P. N.; Dasgupta, A.; Kumar, P. G. V. Plasmofluidic Single-Molecule Surface-Enhanced Raman Scattering from Dynamic Assembly of Plasmonic Nanoparticles. *Nat. Commun*. **2014**, *5*, 4357.

(62) Jin, C.M.; Lee, W.; Kim, D.; Kang, T.; Choi, I. Photothermal Convection Lithography for Rapid and Direct Assembly of Colloidal PlasmonicNanoparticles on Generic Substrates. *Small* **2018**, *14*, 1803055.

(63) Liu, Y.; Huang, Z.; Zhou, F.; Lei, X.; Yao, B.; Meng, G.; Mao, Q. Highly Sensitive Fibre Surface Enhanced Raman Scattering Probes Fabricated Using Laser Induced Self Assembly in a Meniscus. *Nanoscale* **2016**, *8*, 10607-10614.

(64) Mahdy, M. R. C.; Zhang, T.; Danesh, M.; Ding, W. Substrate and Fano Resonance Effects on the Reversal of Optical Binding Force Between Plasmonic Cube Dimers. *Scientific Reports* **2017**, *7*, 6938.

(65) Satter, S. S.; Mahdy, M. R. C.; Ohi, M. A. R.; Islam, F.; Rivy, H. M. Plasmonic Cube Tetramers over Substrates: Reversal of Binding Force as the Effect of Fano Resonance and Light Polarization. *The Journal of Physical Chemistry C* **2018**, *122*, 20923-20934.

(66) Xia, Y.; Whitesides, G. M. Soft Lithography. *An. Rev. Mat. Sci.* **1998,** *28*, 153–184.

(67) Jonáš, A.; Pilát, Z.; Ježek, J.; Bernatová, S.; Fořt, T.; Zemánek, P.; Aas, M.; Kiraz, A. Thermal Tuning of Spectral Emission from Optically Trapped Liquid-Crystal Droplet Resonators. *JOSA B* **2017**, *34*, 1855–1864.

(68) Pilát, Z.; Bernatová, S.; Ježek, J.; Kirchhoff, J.; Tannert, A.; Neugebauer, U.; Samek, O.; Zemánek, P. Microfluidic Cultivation and Laser Tweezers Raman Spectroscopy of *E. coli* under Antibiotic Stress. *Sensors* **2018**, *18*,1623.

ToC Graphic